Carbonization of a Custom Di(trimethylolpropane) tetra-acrylate Photoresist and the Effects of Oxygen Stabilization Process

Qinchen Lin

A thesis

submitted in partial fulfillment of the

requirements for the degree of

Master of Science

University of Washington

2021

Committee:

Eleftheria Roumeli

Lucas Meza

Program Authorized to Offer Degree:

Materials Science and Engineering

University of Washington

Abstract

Carbonization of a Custom Di(trimethylolpropane) tetra-acrylate Photoresist and the Effects of Oxygen Stabilization Process

Qinchen Lin

Chair of the Supervisory Committee:

Prof. Eleftheria Roumeli

Department of Materials Science and Engineering

Glassy carbon has been extensively studied and used in various industrial applications in the last two decades. The versatility comes from its extraordinary mechanical properties, biocompatibility, high chemical resistance & thermal stability, and low electrical resistance. Glassy carbon can be produced from heat treatment of certain polymers beyond their degradation temperature in absence of oxygen (pyrolysis). Though it usually requires pyrolysis at > 2000°C to obtain glassy carbon from bulk polymers with high purity, recent reports show a lower pyrolysis temperature (eg. 900°C) is sufficient to achieve glassy carbon features in micro/nanoscale. This thesis report will focus on the carbonization process (< 1000 °C) on a custom photoresist, a di(trimethylolpropane) tetra-acrylate polymer, in both bulk scales (millimeter) and micrometer scales. The effects of pre-pyrolysis oxidation (<350 °C) on the

carbonization process are also investigated. Our findings show that in the case of bulk samples, the pre-pyrolysis oxidation process can improve the final yield of the carbon products.

Table of Contents

List of Figures

List of Tables

Acknowledgments

First, I would like to express my greatest gratitude to my supervisor Prof. Eleftheria Roumeli who provided me with this wonderful research opportunity and guided me through the project. It wouldn't be possible to accomplish this thesis without her mentorship and endless support. I would also like to express my sincere appreciation to another committee member Prof. Lucas Meza for his time and valuable feedback. Thank you to my fellow lab members, Dr. Andrew Jimenez, Amanda Inthavong, Mallory Parker, and Konstantina Mason for their valuable contributions to this thesis. I would also like to thank the other members of the Roumeli group for their important feedback. Last but not least, I would like to thank my family for their love, encouragement, and support.

Chapter 1 – Background

1.1. Pyrolysis, Different Carbon products, and Common Characterization Methods

The concept of pyrolysis is well discussed in Sharma's review [1]. It's a heat treatment on organic materials in absence of oxygen. Some applications include the chemical vapor deposition of graphene (gas-phase pyrolysis) [2], the waste polymer treatment[3][4], and the fabrication of ultra-strong carbon nanostructures [5][6][7]. This thesis only focuses on the pyrolysis process that converts polymers to carbon products, particularly glassy carbon. When polymers undergo heat treatment beyond their degradation temperature, the breaking of carbon-heteroatom bonds enables the formation of new carbon-carbon bonds [8]. At the early stages of the pyrolysis process, different hydrocarbon radicals are produced and reach the highest concentration at 600 °C [9]. A graphene network, which contains a large fraction of defects and chemical impurities, starts to develop after 800 °C [10]. Further heat treatment can increase the graphene crystallite size (L_a) and stack thickness (L_c) through annealing the defects [1]. In Fig. 1.1 a schematic that explains the structure and crystallinity changes for precursor molecules during heat treatment is presented [11]. The transformation chain for different precursors is not necessarily the same as is shown in Fig 1.1 due to different bonding, networking capabilities, and defects in graphitic and non-graphitic phases [12]. For example, some precursors can lead to non-graphitizing products that can't be converted to crystalline graphene even with high temperatures. It should also be noted that the graphitic and non-graphitic phases in Fig 1.1 are transformation phases during pyrolysis, which should be distinguished from graphitizing/non-graphitizing carbons that describe the final carbon products. Besides the choice of precursors [13], structure sizes [13], applied force [14], and heating conditions [13] can affect

the nature of the final carbon products as well.

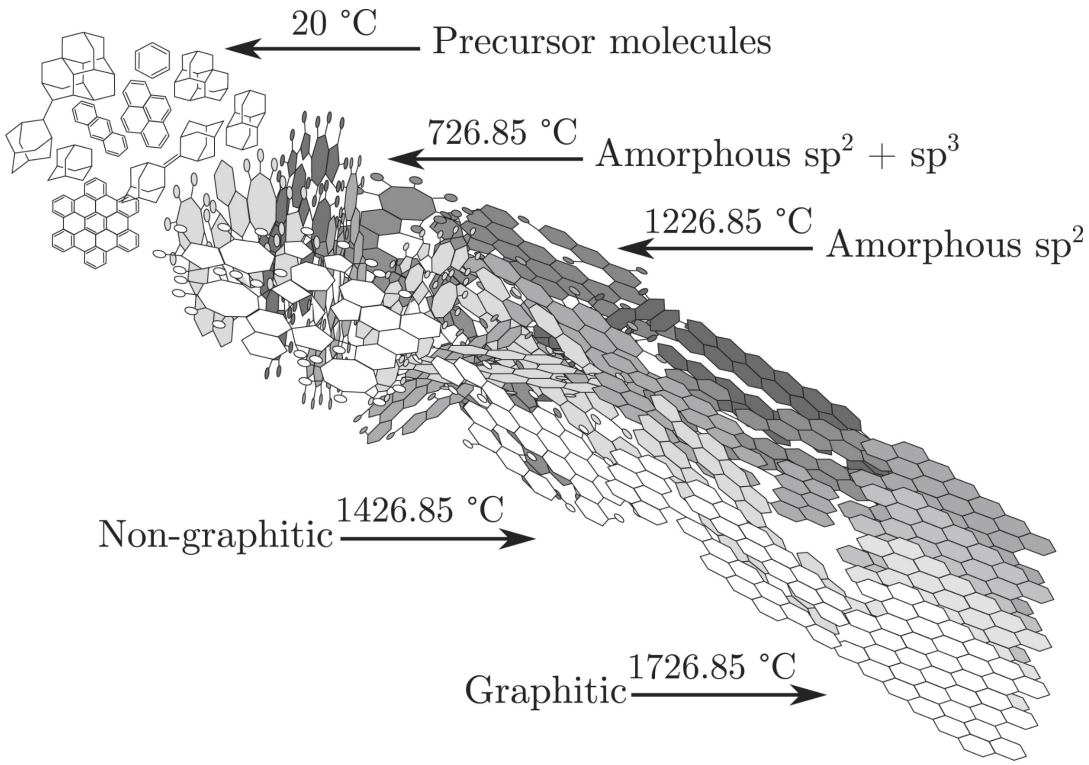

Fig 1.1. Change of structural units and crystallinity of precursor molecules during heat treatment. Adapted from [11].

Some commonly used characterization methods of carbon products include Raman Spectroscopy[7][12][15], X-ray Diffraction (XRD) [16][17] (both of which can be non-destructive), and Transmission Electron Microscopy (TEM) [10][15][18] (which is destructive). As Raman Spectroscopy is the main characterization method used in this work, the concept and typical uses of Raman spectra for carbon products are discussed. Raman spectroscopy is a non-destructive characterization method. It shines a light source, usually laser, onto a sample and detects inelastic scattering (Raman scattering) from the interaction of laser light and molecules' vibration modes, which gives the information of the samples' molecular structure [19][20]. For carbon products, the D band (around $1350\ cm^{-1}$) and G band (around

1600 cm^{-1}) in Raman spectra are of particular interest. The G band peak is associated with an in-plan stretching of sp^2 bond carbon atoms. The D band is a disorder-induced band, which doesn't present in perfect crystalline graphene [21]. For carbon products with a large graphene crystallite size (L_a), the D band intensity mainly corresponds to defects or disorders. So the decrease in D band intensity with respect to the G band indicates an increase in order. For example, Fig 1.2(a) shows Raman spectra of graphitizing carbon at different temperatures. In those spectra of carbon products with pyrolysis temperature > 1500°C (large L_a), the D band intensity decreases with respect to the G band as defects are annealed. However, for carbon products with small L_a, such as amorphous carbon and disorder carbon, the D band strength mainly corresponds to the breathing mode vibration of 6-fold aromatic carbon rings [15]. In this case, the increase of D band strength is a sign of ordering [22]. This can be seen in Fig 1.2(b), Raman spectra of non-graphitizing carbon, and also lower temperature region (<1500°C, small L_a) in Fig 1.2(a), graphitizing carbon.

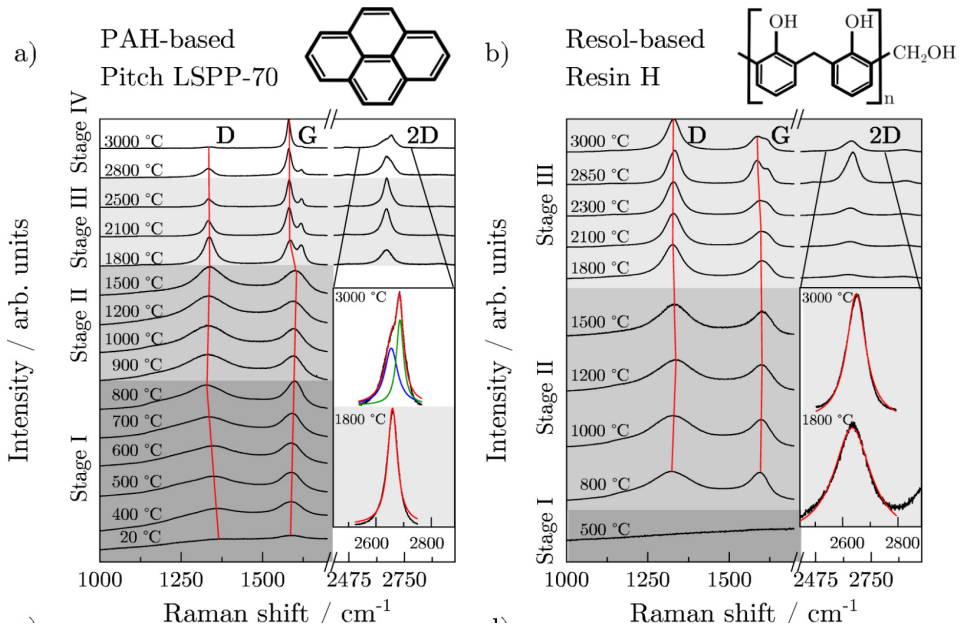

Fig 1.2. Raman spectra of graphitizing (a) and non-graphitizing carbon products (b) obtained from the pyrolysis of two different precursors at different temperatures. Adapted from [12].

There are empirical models available to determine L_a. From the work done by Tuinstra and Koenig [23], the peak intensity ratio of the D band and G band is proportional to $1/L_a^2$ for graphite. As Ferrari and Robertson showed, in amorphous and disordered carbons, the development of the D peak strength is a sign of ordering [22]. They also proposed a new formula for carbon products with small L_a (< 20 Å), I(D)/I(G) ~ L_a. In this work, the absolute intensity without any peak fittings was used for the I(D)/I(G) ratio. Because no fittings on spectra were done, the peaks ratios were only used to make comparisons among different intermediate / final products obtained from pyrolysis, and not for determining L_a. Graphene crystallite size could be determined by XRD [16][17] and the ultrastructure of products could also be studied through TEM [10][15][18], but that was not conducted in the present work.

1.2 Glassy Carbon

Glassy carbon is a type of non-graphitizing carbon, which cannot be converted to crystalline graphite due to its randomly oriented graphene fragments, large interlayer separation, and misaligned basal planes [1]. Glassy carbon has been extensively studied and used in various industrial applications in the last two decades [1]. The versatility comes from its extraordinary mechanical properties, biocompatibility, high chemical & thermal resistance, and low electrical resistance. Some properties of commercially available bulk glassy carbon are given in Table 1.1.

Table 1.1. Properties of glassy carbon in bulk scale [1]

Properties	Values	Reference
Young's modulus	20 - 40 GPa	[24][25]
Poisson's ratio	0.15 - 0.17	[24]
Density	1.3 - 1.55 g/cm^3	[26]
Electrical resistivity	10–50 μΩm	[26]
Thermal expansion coefficient	(2.0–3.4) × 10^{-6} K^{-1}	[27]

Glassy carbon can be produced by the heat treatment of certain polymers beyond their degradation temperature in absence of oxygen (pyrolysis). Some of the well-known glassy carbon precursors such as Phenol-formaldehyde (PF) resins are widely used to make different commercially available photoresists due to their thermosetting character, various viscosities, and capability of facilitating a chemical amplification after the photoacid generation [28][29]. Other resists such as acrylate-based polymer are also used in nano-scale fabrication, and their conversion to glassy carbon further improves their mechanical performance as well as other physical and chemical properties [30]. Even though a pyrolysis treatment at >2000 °C is usually required for bulk samples, millimeter-scale, to be converted to glassy carbon with high purity [31], it has been reported that the glassy carbon features can also be achieved in micro/nanostructures at lower temperature (eg. 900 °C) [5][6][7]. The pyrolysis process for micro/nanostructures usually involves multiple steps heating and isothermal processes, which

will be discussed in section 1.4. Some of those resists, even with well-known glassy carbon precursors, may give none or small amounts of carbon products after pyrolysis, which can result in different properties compared with glassy carbon [1]. As a result, careful evaluations are necessary for new custom resists. This thesis will focus on the carbonization of our custom photoresist, an acrylate-based polymer, and the characterization of the intermediate & final products.

1.3. Oxygen stabilization

Oxygen stabilization is a pre-pyrolysis heating process under an oxygen-containing environment, which is usually done at lower temperatures (eg. 300 °C). This process has been extensively studied for carbon fiber production by pyrolysis of cellulose, polyacrylonitrile (PAN), or other polymer fibers [32][33][34]. In the case of PAN fibers, the studies show that the oxygen stabilization prior to the carbonization process is crucial to prevent the melting or fusion of the fibers and minimizes volatilization of elemental carbon in the following carbonization step, which maximizes the final yield of carbon fibers [33]. It has also been reported that the pre-pyrolysis oxidation on PAN fibers can strongly affect the properties of the final products [35]. Since polymer fibers and polymeric micro/nanostructures share a high surface-to-volume ratio, the main hypothesis of this thesis was that their annealing patterns and pyrolysis process could be similar. The effects of oxygen stabilization on the carbonization process of di(trimethylolpropane)tetra-acrylate photoresists will be discussed in this work.

1.4. Two-photon Lithography (TPL)

The concept of two-photon lithography (TPL) is well discussed in the literature [36]. Two-photon lithography is one of the direct laser writing techniques that has been frequently used for 3D microstructures manufacturing due to its high spatial resolution and dimensional accuracy [37]. Among different laser-based writing techniques, two-photon lithography (TPL) is particularly successful in producing well-defined 3D micro/nanostructures because it enables the possibility to have a spatial resolution beyond the diffraction limit [38]. This advanced technique is based on two-photon polymerization. When photon energy is provided to a liquid resin, it can be converted to solid through crosslinking or photon-polymerization [36]. For TPL, the resin absorbs two photons at the same time and results in a non-linear process, and hence, the polymerization rate and light intensity have quadratic dependence [39], which allows high 3D spatial resolution and accuracy compared with conventional single-photon lithography [36]. Another advantage of TPL is that materials absorb two photons at a longer wavelength, usually in near-infrared religion (NIR), and the linear absorption of the light in NIR for most commercially available polymers is negligible [36]. As a result, the laser beam can penetrate the liquid resin and induce the polymerization from a point inside a bulk. Schematics of the nonlinear absorption and TPL process are shown in Fig 1.3 and Fig 1.4.

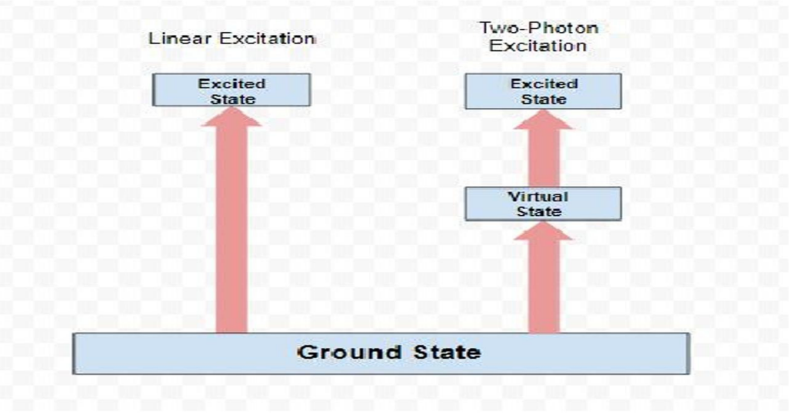

Fig 1.3. Schematic of nonlinear absorption, adapted from [40].

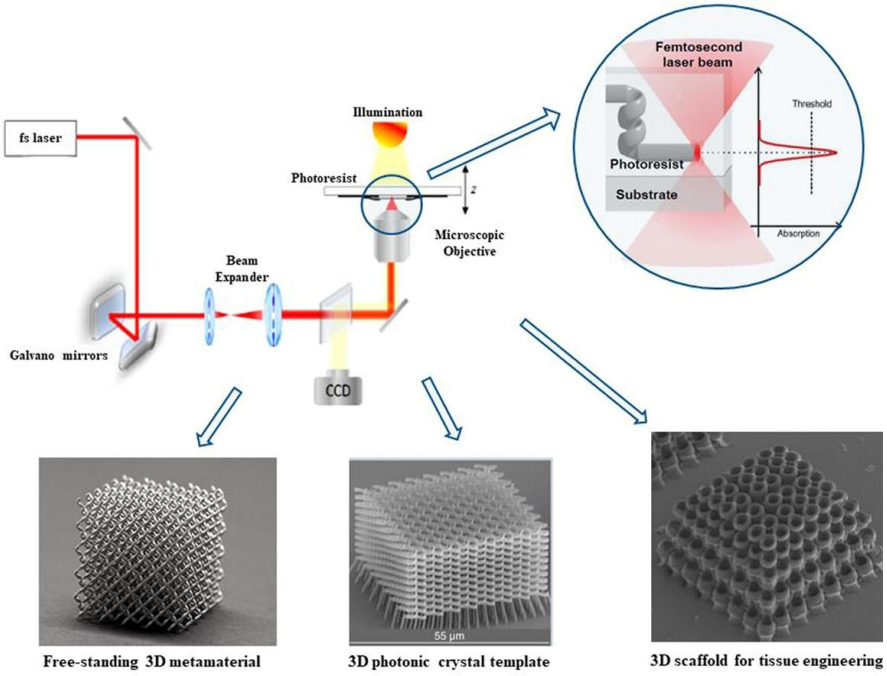

Fig 1.4. Schematic of the two-photon lithography process, adapted from [40].

1.5. Combination of TPL and Pyrolysis

Though TPL is capable of printing well-defined 3D micro/nanostructures, a resolution below 100 nm can't be achieved [41]. Another limitation is that the polymeric resists required for the lithographic process have much lower stiffness and strength compared with ceramic materials [5]. To overcome those limitations, the combination of 3D direct laser writing and pyrolysis is a possible solution. Pyrolysis of micro/nanostructures printed by 3D direct laser writing (TPL process) allows the further reduction in size beyond the limitation [5][6][7] to meet the growing interest of 3D nanostructures (sub-100nm). With volumetric shrinkage up to 90% [42], polymer micro/nano-structures can turn into carbon nanostructures, usually glassy carbon, while the pre-patterns are preserved. Furthermore, the mechanical properties are enhanced after pyrolysis, see section 1.2 for more information on mechanical properties of glassy carbon. For example, it has been reported that for lightweight glassy carbon nanolattices with a honeycomb structure obtained from pyrolysis of micro lattices, Fig 1.5, an extraordinary strength to density ratio (1.2 Gpa at $0.6\,cm^{-3}$) was achieved [5]. This value is close to the lower bond of the theoretical limit and better than any bulk metallic, polymeric, and composite materials, as well as most technical ceramics, leaving diamond the only bulk material that has a better performance [5].

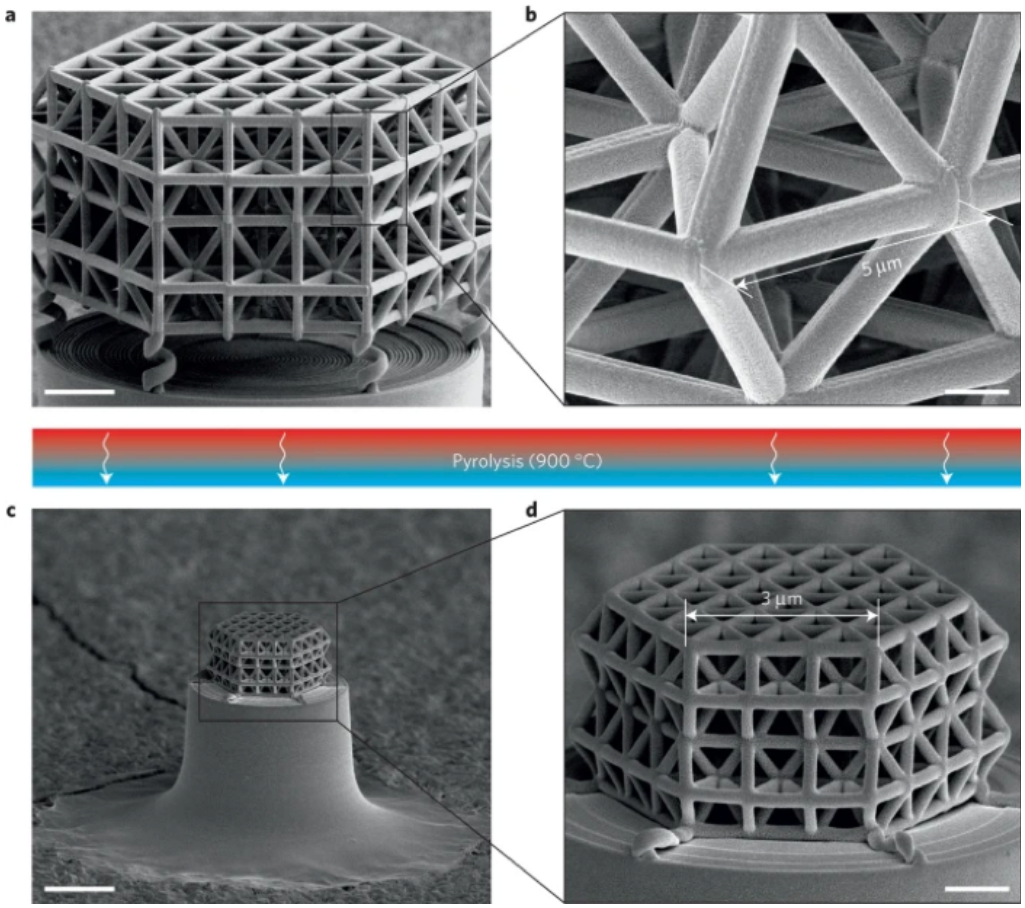

Fig 1.5. Honeycomb polymeric structure before and after pyrolysis. Adapted from [5].

Besides the extraordinary mechanical properties, the excellent chemical resistance & thermal stability, electrical conductivity, and biocompatibility of glassy carbon, combining with the possible complex geometries obtained from pyrolysis of pre-patterned micro/nano polymeric structures allow the development of new opportunities in various nanotechnology industries. Applications that have been reported include microelectrodes [43][44], micro/nanowires [45][46], microneedles [47], metamaterials [5][6], among others.

Chapter 2 – Materials & Methods

2.1. Monomer and Initiator

The liquid resin consists of Di(trimethylolpropane) tetraacrylate as monomer and 2-Benzyl-2-(dimethylamino)-4′-morpholinobutyrophenone as photoinitiator with a mass ratio of 100:1. The molecular structures are shown in Fig 2.1 and Fig 2.2.

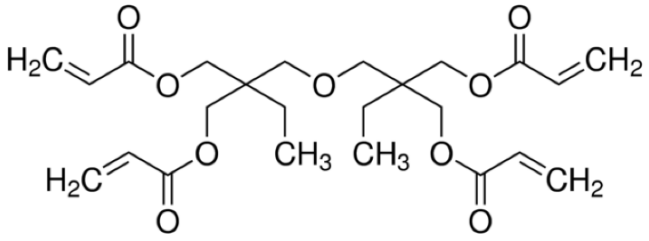

Fig 2.1. Molecular structure of Di(trimethylolpropane) tetra-acrylate

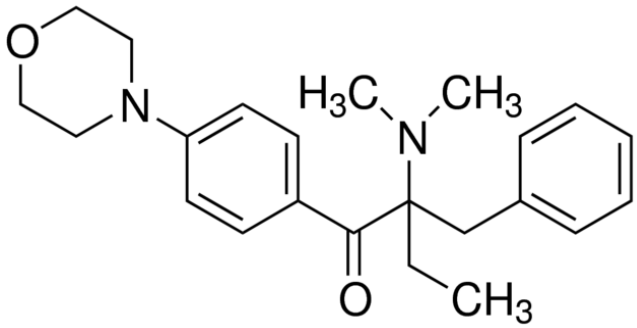

Fig 2.2. Molecular structure of 2-Benzyl-2-(dimethylamino)-4′-morpholinobutyrophenone

2.2. Bulk Samples and Micropillars

For bulk samples, the liquid resin was spread on a glass slide and cured by a high-intensity UV lamp (BlueWave 200, Dymax, USA) with a 300 - 450 nm emission spectrum (Fig. 2.3). A study predating this work was conducted to determine the amount of time required

for this resin in bulk form to reach the saturated DOP. The DOPs of Bulk films that were cured under a high-intensity UV lamp for 1 min, 5 mins, 10 mins, 30 mins, and 60 mins were calculated using Raman data, which shows that only 1 min exposure is sufficient to cure the liquid resin with saturated DOP. However, the bulk film with 60 mins UV exposure was used in this work to ensure the sample has maximum DOP. The bulk film (thickness varies from 0.28mm to 0.61mm) was cut into multiple bulk samples of 6mm x 6mm square shapes (Fig. 2.4) in order to fit in the thermogravimetric analysis (TGA) sample pan. The mass of bulk samples was in the range of 5mg to 7mg.

Fig 2.3. High-intensity UV lamp in Washington Nanofabrication Facility (WNF).

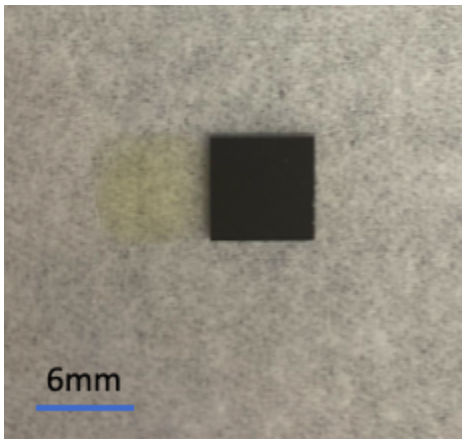

Fig 2.4. Bulk polymer sample (left) and a 6mm x 6 mm silicon substrate (right)

Polymeric micropillars with a target aspect ratio of 2 were printed by a Photonic Professional GT (Nanoscribe GmbH) direct laser writing system (Fig. 2.5), using a Plan-Apochromat 63 × 1.4 Oil DIC M27 (Carl Zeiss AG) objective and a FemtoFiber pro-NIR (TOPTICA Photonics AG) laser, with a center wavelength (λ) of 780 nm, a pulse width (τ) of ≈ 100 fs, and a repetition rate (f) of 80 MHz. The choice of micropillar fabrication parameters is given in Table 2.1. Using a sequential design of a silicon wafer (6mm x 6mm), a set of spacers and a resin droplet filling the volume between them, followed by a transparent coverslip, a total of three 5 x 5 arrays of micropillars (one array for each micropillar set with diameters of 10µm, 25µm, and 50µm) were printed. After printing, the wafer was cleaned in propylene glycol monomethyl ether acetate (PGMEA) solution for 5 mins, IPA for 5 mins, and ultra-pure IPA for 10 mins. During the ultra-pure IPA immersion, the samples were exposed to a UV lamp with an on-and-off procedure (30s on and 30s off) for a total duration of 5 minutes. Then the samples were dried in a critical point dryer (CPD), and a final exposure to the UV lamp was applied for another 5 minutes.

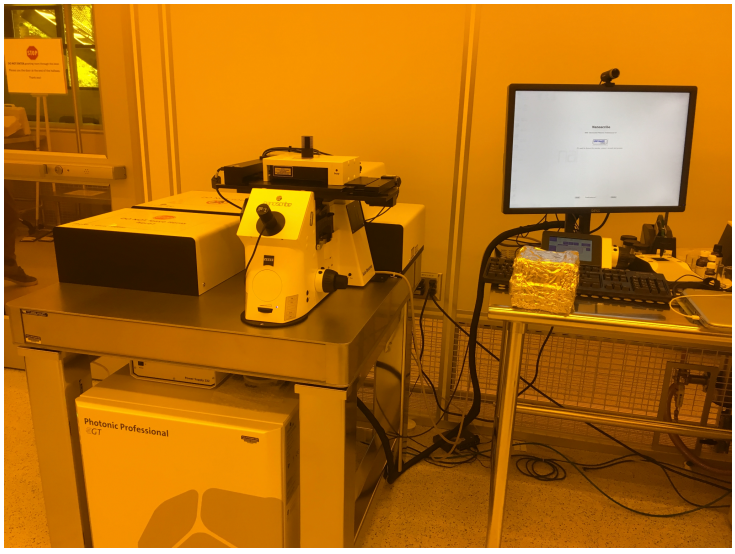

Fig 2.5. Photonic Professional GT system at WNF.

Table 2.1. Printing parameters for micropillars with different diameters.

Diameters	Laser Power (%)	Scanning Speed (mm/s)
10μm	53	8000
25μm	80	5500
50μm	80	7000

2.3. Characterization Methods

2.3.1. Raman Spectroscopy

Fig 2.6. Raman Spectroscopy in Molecular Analysis Facility (MAF), University of Washington.

The Raman Spectroscopy at Molecular Analysis Facility (MAF) in University of Washington, Fig 2.6, with a Reinshaw InVia Raman Microscope (Renishaw, Wotton-under-Edge, United Kingdom) was used for calculating the DOP of cured photoresists before pyrolysis and

the characterization of the intermediate/final products after pyrolysis. The system is equipped with an inVia Spectrometer, a Leica DM IRB microscope, and a set of high-power lasers (785 and 514 nm). All spectra fittings were done on the Renishaw WIRE software. Baseline subtraction was done using 5th order polynomial fitting, Fig 2.7.

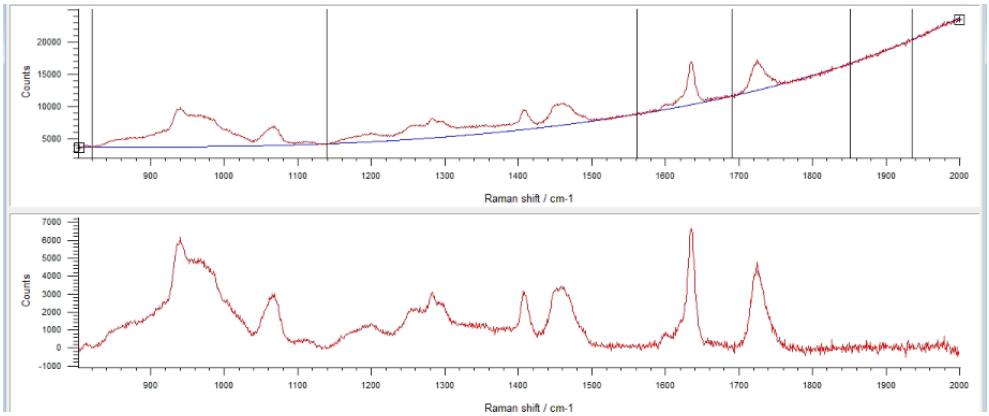

Fig 2.7. Renishaw WIRE software baseline subtraction example.

To measure the DOP of cured photoresists, a 785 nm excitation laser, a 50X objective (0.5mm working distance), 50 percent laser power, and 10 seconds accumulation time were chosen to obtain the spectra of the solidified polymer. For liquid resin, a 10X objective with a longer working distance (11 mm) was used to avoid damaging the objective. The DOP was determined by measuring the relative change of the integrated area of C=C peak (at about 1635 cm^{-1}) with respect to C=O peak (at about 1725 cm^{-1}) of the liquid resin before/after polymerization using the following formula [48][49] :

$$DOP\ \% = 1 - \frac{\frac{A_{C=C}}{A_{C=O}}}{\frac{A_{C=C}^{resin}}{A_{C=O}^{resin}}} \times 100$$

For the peak fitting, the Voigt function (Gaussian/Lorenzo) was used, Fig 2.8.

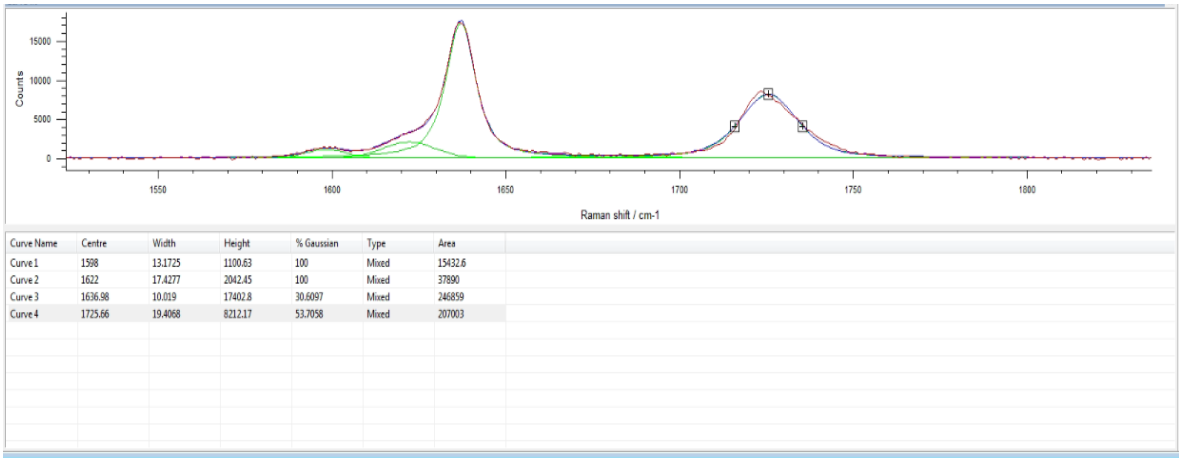

Curve Name	Centre	Width	Height	% Gaussian	Type	Area
Curve 1	1598	13.1725	1100.63	100	Mixed	15432.6
Curve 2	1622	17.4277	2042.45	100	Mixed	37890
Curve 3	1636.98	10.019	17402.8	30.6097	Mixed	246859
Curve 4	1725.66	19.4068	8212.17	53.7058	Mixed	207003

Fig 2.8. Spectrum fitting example.

To characterize the intermediate products from the pyrolysis/oxidation process, the same excitation laser and objective (785 nm laser and 50X objective) as those for solidified polymers were used so that it's easier to compare the spectra. As for the final carbon products, a 514 nm excitation laser and 50X objective were used because green lasers are more commonly used for carbon products [7][22][10].

2.3.2. Thermogravimetric Analysis (TGA)

TGA measurements were conducted in a D550 from TA Instruments (New Castle, DE). Samples were heated following each of the described heating profiles in the Results & Discussion section at a heating rate of 2.5°C/min in either N_2 or air with the same flow rate of 60 mL/min. The flow rate for balance purge (N_2) is 40 mL/min.

Fig 2.9. TGA 5500

2.3.3. Scanning Electron Microscopy (SEM)

SEM images were obtained using an EBSD - Apreo SEM (ThermoFisher Scientific, Waltham, MA) operating typically at a voltage of 2kV and a current of 13pA. All samples in polymer form were first coated with a 4nm layer of Platinum, while pyrolyzed products were images without any treatment.

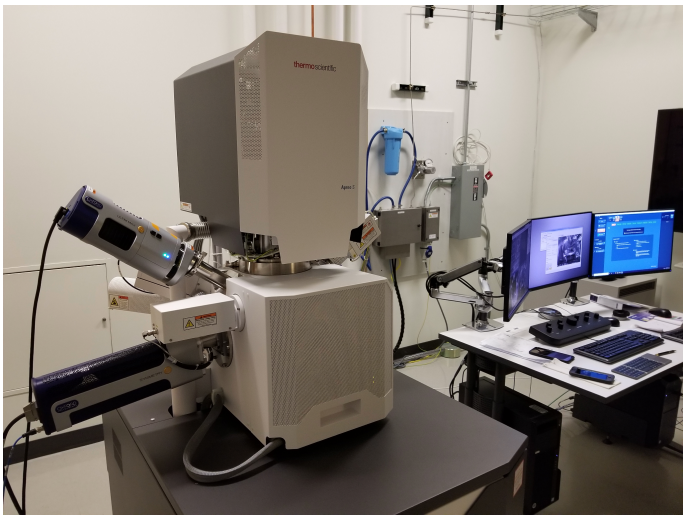

Fig 2.10. Electron Back-Scatter Diffraction (EBSD) SEM in MAF.

Chapter 3 – Results & Discussion

3.1. Degree of Polymerization

Before any heat treatments are applied to the samples, the degree of polymerization was determined by using Raman spectroscopy, following the analysis described in section 2.3.1. By taking the average values of 5 spots (5 pillars in the case of micropillars), Fig 3.1, the average degree of polymerization for the bulk sample is 44.96%. The average DOPs of micro-pillars with diameters of 10µm, 25µm, and 50µm are 31.62%, 33.57, and 35.79 respectively. A significant difference in DOP between bulk samples and micropillars may be due to the size effects or the different polymerization processes (two-photon polymerization versus UV-photopolymerization). The values are similar to the DOPs of other acrylic-based resins, such as IP-L780, used by other groups [48][49].

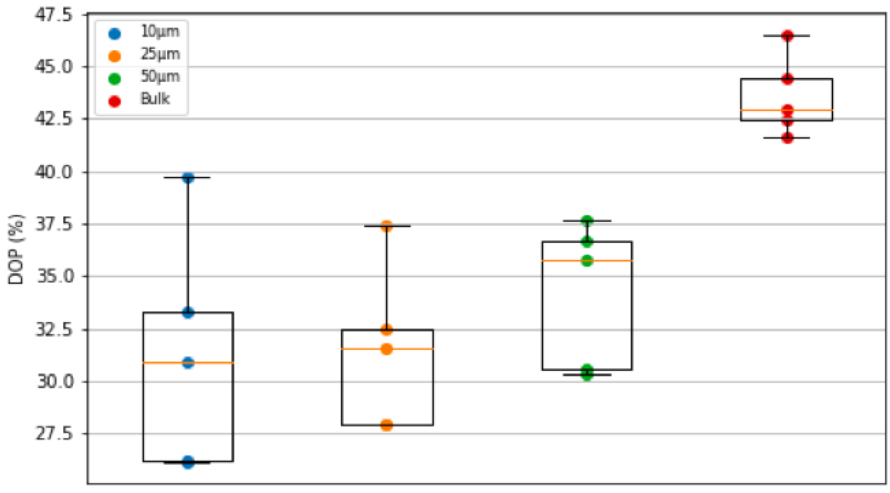

Fig. 3.1. Degree of polymerization for both bulk samples and micropillars with different diameters.

3.2. Single-Step Heating

Heat treatments without any isothermal process were done on bulk samples in a TGA furnace. Bulk samples were heated from room temperature to 900°C with a ramp rate of 2.5°C / min both in air and in nitrogen gas. The final yields of carbon products after heat treatments were extremely small, 0.88% (in nitrogen) and 0.17% (in air). From the TGA data, Fig 3.2, the polymer bulk sample starts to lose weight at about 300°C in air. While in nitrogen gas, the weight loss starts to be significant after 350°C. These two temperatures were later used as a starting point to design the multi-step heating process.

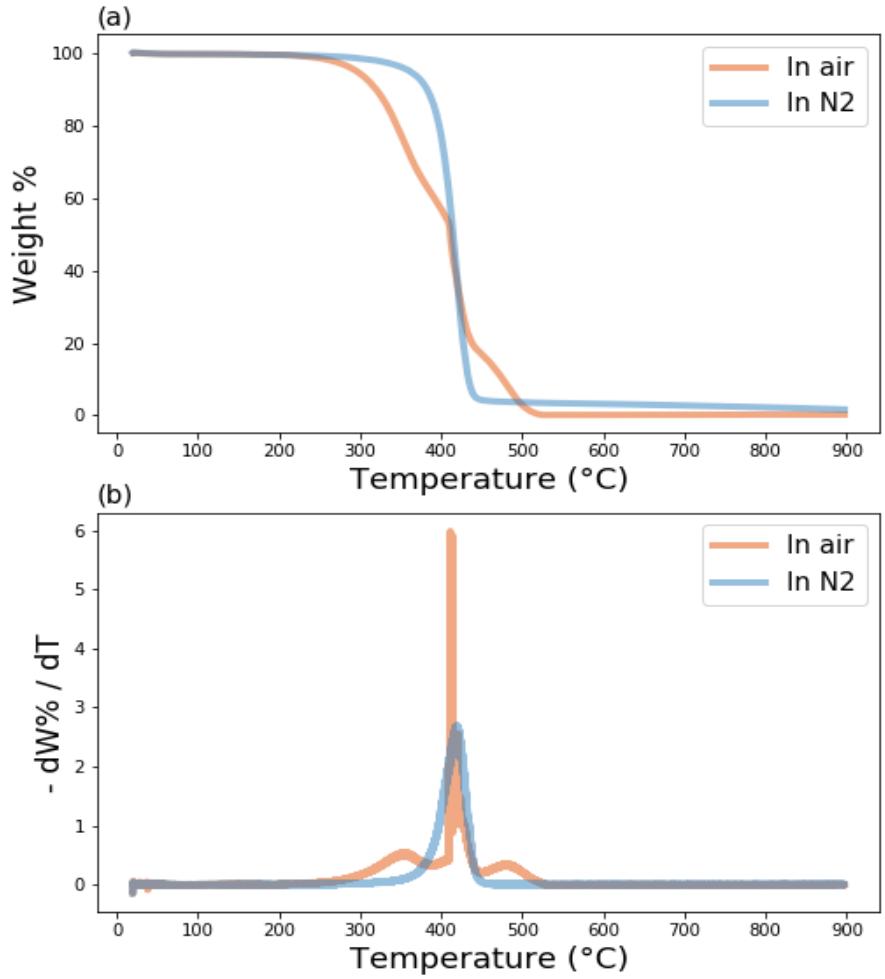

Fig 3.2. TGA data of single-step heat treatments on polymer bulk samples.

3.3. Multi-step Heating Process

Multi-step pyrolysis was used by different groups on polymeric micro/nano-structures printed by 3D direct laser writing (TPL process), where the polymeric structures undergo volumetric shrinkage and turn into carbon nanostructures [5][6][7]. The heat treatments involve two or more isothermal processes. Firstly, the sample is heated to a target temperature, T1 (usually 250°C to 300°C), at some chosen ramp rate. After an isothermal process at T1, the sample is then heated to the final temperature T2 (usually 690°C - 1000°C) followed by another isothermal process. Some groups added more intermediate temperatures and isothermal processes between T1 and T2 [6][7]. The whole process is done in inert gas or vacuum environment. The choice of target temperature, T1&T2, ramp rate, and the time of the isothermal process vary among different groups depending on the materials they used.

In this work, both multi-step pyrolysis (all processes in nitrogen) and the modified process, where step 1 (see Fig 3.3) is done in air (pre-pyrolysis oxidation) were applied to bulk samples. Because there are no previous investigations on the carbonization process of our custom photoresist, the value of T1 was chosen based on the observation from single-step heatings, section 3.2 (the temperatures that polymer bulk samples start to lose mass). The isothermal process of 2 hours was chosen to make sure it's long enough to distinguish the effects of oxygen stabilization. For the rest parameters, values that are close to the choices of other groups were chosen [5][6][7]. The heat treatments (Table 3.1), with/without oxygen stabilization, were applied to bulk samples. To confirm the purity of final carbon products, subsequent heatings from room temperature to 1000°C in nitrogen were also performed. Because the ramp rate of 2.5°C /min and the isothermal process of 2 hours were held fixed throughout all the

experiments, $H_{T1/T2}$ is used to denote different heat treatments. For example, $H_{300/900}$ denotes the heat treatment with T1 = 300°C, T2 = 900°C, i.e. the first row in Table 3.1.

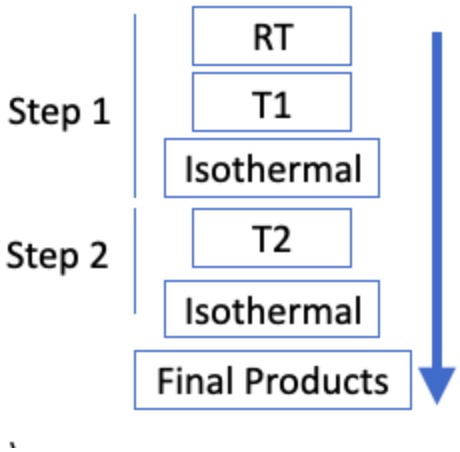

Fig 3.3. Schematic of multi-step pyrolysis.

Table 3.1. Choice of parameters in different heat treatments.

T1 (°C)	T2 (°C)	Isothermal (hours)	Ramp rate (°C/min)
300	900	2	2.5
300	950	2	2.5
350	900	2	2.5
350	950	2	2.5

3.3.1. Multi-step Heating on Bulk Sample

With T1 held fixed to be 300°C, The heat treatments $H_{300/900}$ and $H_{300/950}$ were done in the TGA furnace with/without pre-pyrolysis oxidation process. After being heated to 300°C, the

bulk sample that was heated in air lost more than 20% of weight during the isothermal process while the bulk sample heated in nitrogen gas only lost a small amount of weight, Fig 3.4. The intermediate products were collected from the separate runs with step 1 only (RT - 300°C and held for 2 hours) both in air and in nitrogen, Fig 3.5. The intermediate product with the heat treatment in nitrogen has almost the same color as it was before pyrolysis, and the spectrum is given in Fig 3.6. Compared with the spectrum of bulk polymer before pyrolysis, the decrease in peaks at around 1635 cm^{-1} (corresponds to C=C bond [48]) shows that the carbon double bond starts to break in nitrogen gas at 300°C even with a small mass loss. The intermediate product that was heated in the air appears to be dark red. The spectrum is not provided because the high fluorescence was observed with both 514 nm and 785 nm lasers, which masks the Raman signal.

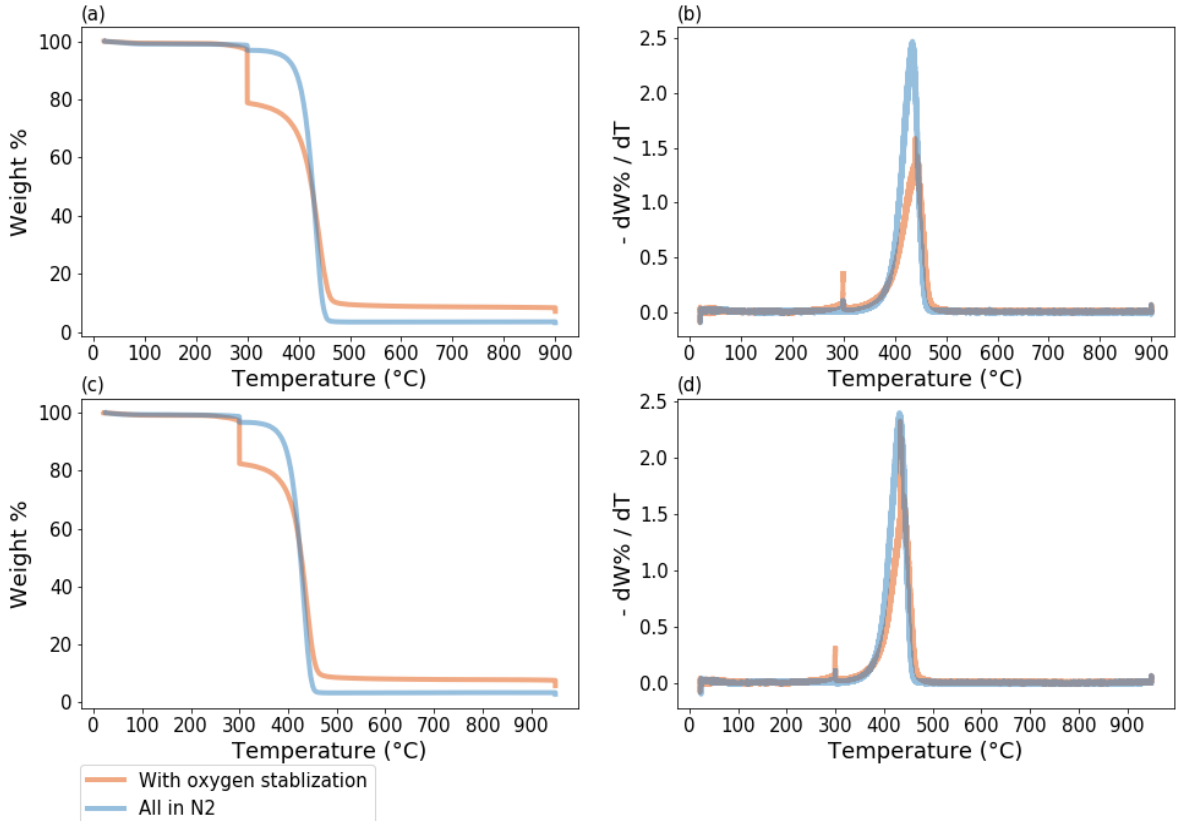

Fig 3.4. TGA data of multi-step heating process with/without oxygen stabilization on polymer bulk samples. (a) and (b): $H_{300/900}$, (c) and (d): $H_{300/950}$.

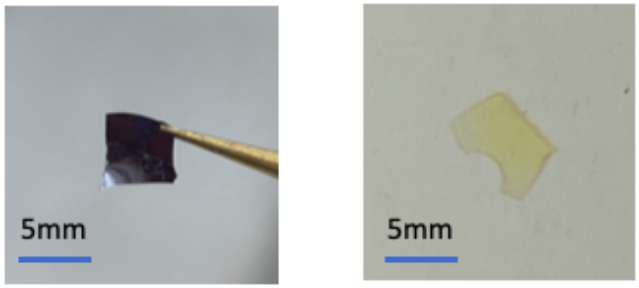

Fig 3.5. Intermediate products obtained from a separate run with step 1 only (RT - 300°C - 2h isothermal process). Left: in air. Right: in nitrogen.

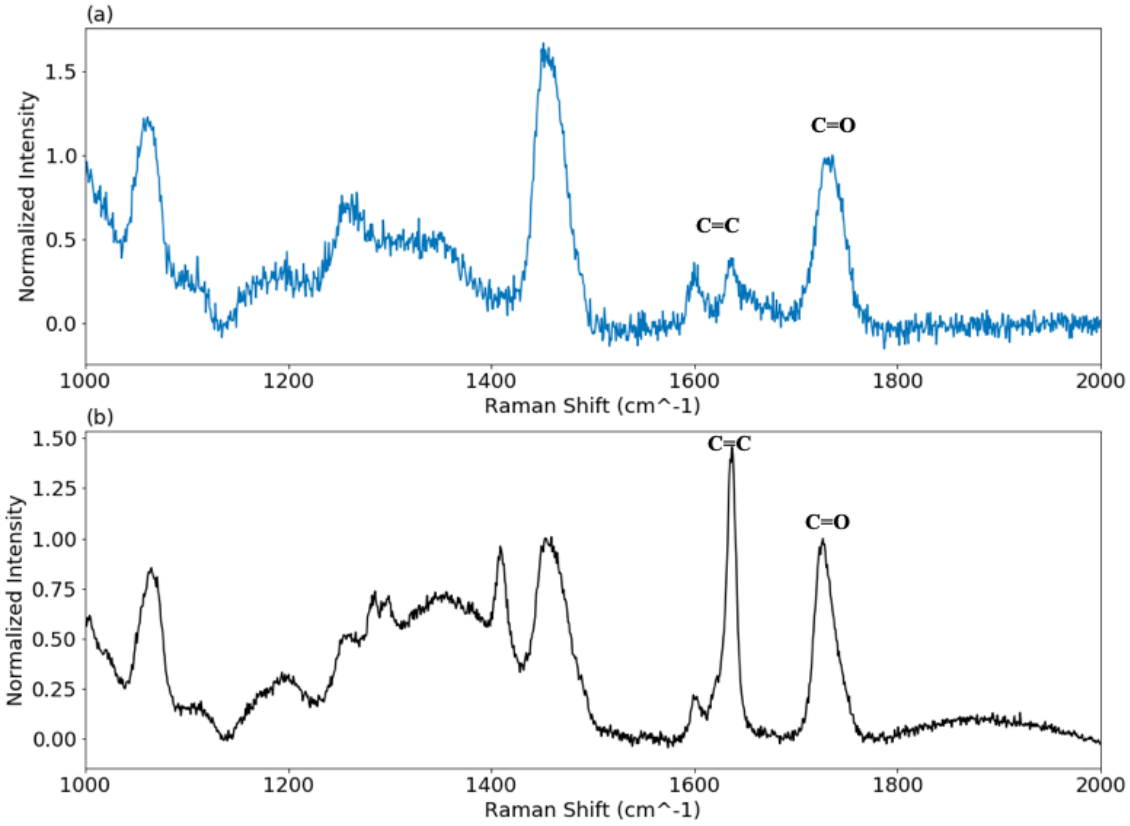

Fig 3.6. Normalized (G band peak intensity = 1) Raman spectra for intermediate products (a) after step1 pyrolysis (RT - 300°C - 2 hours isothermal process) and bulk polymer sample before pyrolysis (b).

After full heat treatment, for both $H_{300/900}$ and $H_{300/950}$, the final products with/without pre-pyrolysis oxidation have noticeable differences in terms of the weight and the size, Fig 3.4

and Fig 3.7, which shows that the pre-pyrolysis oxidation improves the final yield. To confirm the glassy carbon features of the final products, Raman spectroscopy was used for characterization, Fig 3.8. From the Raman spectra, for both $H_{300/900}$ and $H_{300/950}$, glassy carbon features can be seen [7][15], with no significant differences between the final products with/without pre-pyrolysis oxidation.

Fig 3.7. Final carbon products obtained from $H_{300/900}$. Left: without pre-pyrolysis oxidation (all processes were done in nitrogen). Right: with pre-pyrolysis oxidation.

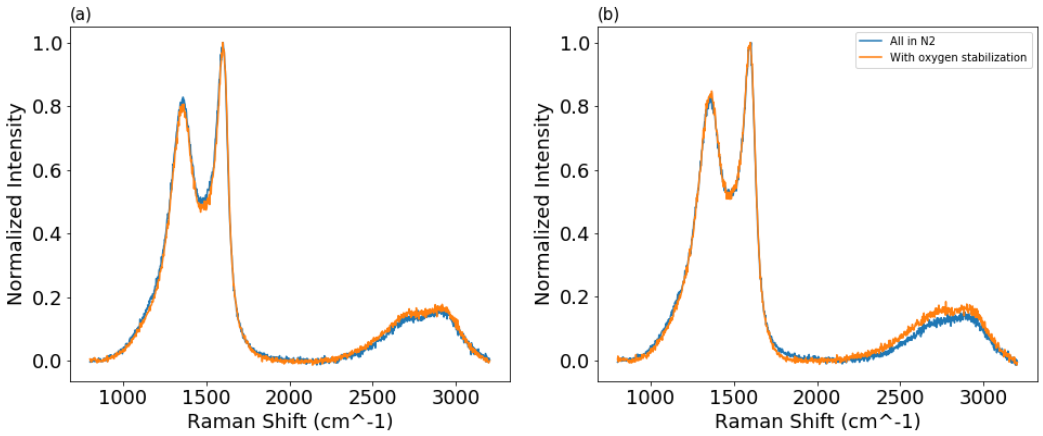

Fig 3.8. Normalized Raman spectra (G band peak intensity = 1) of the carbon final products. (a): $H_{300/900}$, (b): $H_{300/950}$.

Increasing T1 to 350°C, heat treatments $H_{350/900}$ and $H_{350/950}$ were performed in the TGA furnace with/without pre-pyrolysis oxidation process. With higher T1, the bulk sample heated in nitrogen started to lose a noticeable amount of mass (about 14%) while the sample

heated in air lost a significant amount of mass (more than 40%). The intermediate product was collected from a separate run with step 1 only (RT - 350°C - 2h isothermal process), Fig 3.10. With the step 1 heat treatment in air, the polymeric bulk sample turned into a shiny black color, and the Raman spectrum is given in Fig 3.11. From the spectra, clear D and G bands can be observed, which shows the carbon features with some disorder. The intermediate product that was heated in nitrogen appears to be brown. The Raman spectrum is not given because of high fluorescence.

Similar to heat treatments $H_{300/900}$ and $H_{300/950}$, the final yield of the carbon products from $H_{350/900}$ and $H_{350/950}$ with oxygen stabilization process appears to be improved, Fig 3.9, while the Raman spectra, Fig 3.12, show that the oxygen stabilization process doesn't change much on the quality of the final carbon products.

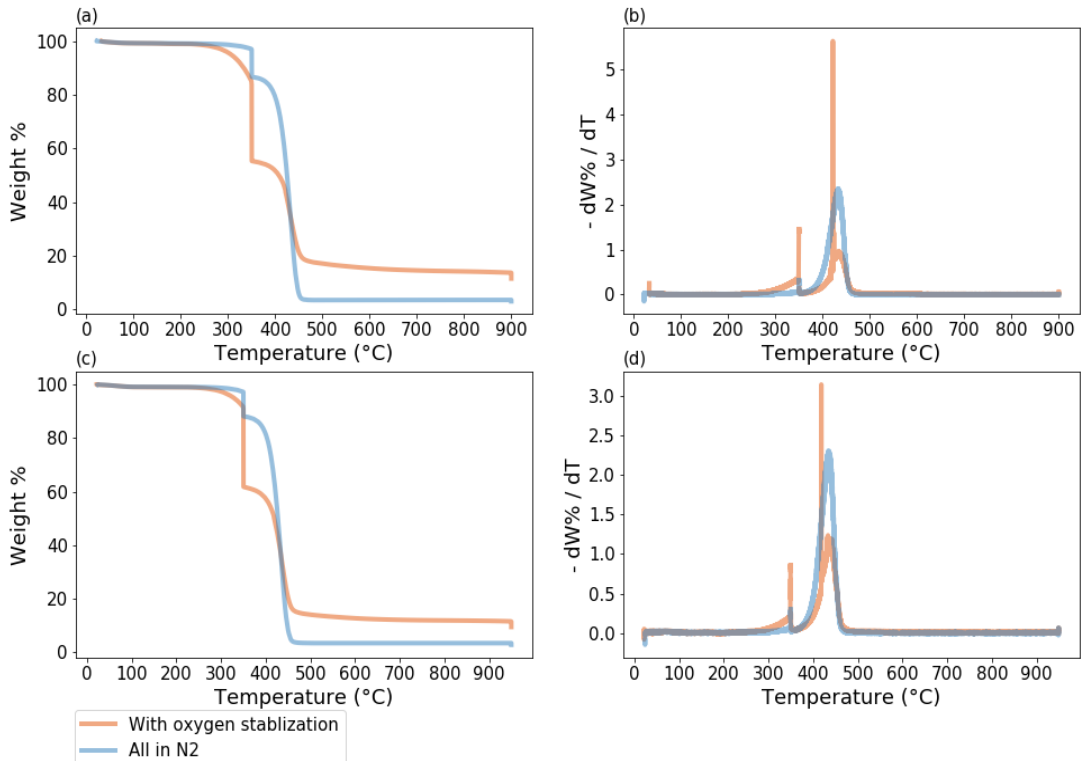

Fig 3.9. TGA data for multi-step heating with/without oxygen stabilization on polymer bulk samples. (a) and (b): $H_{350/900}$. (c) and (d): $H_{350/950}$

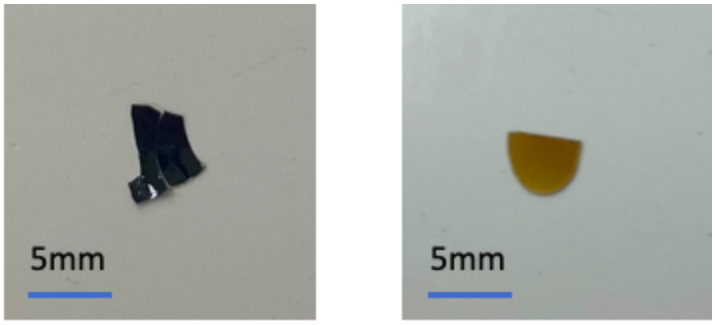

Fig 3.10. Intermediate products obtained from a separate run with step 1 only (RT - 350°C - 2h isothermal process). Left: in air. Right: in nitrogen.

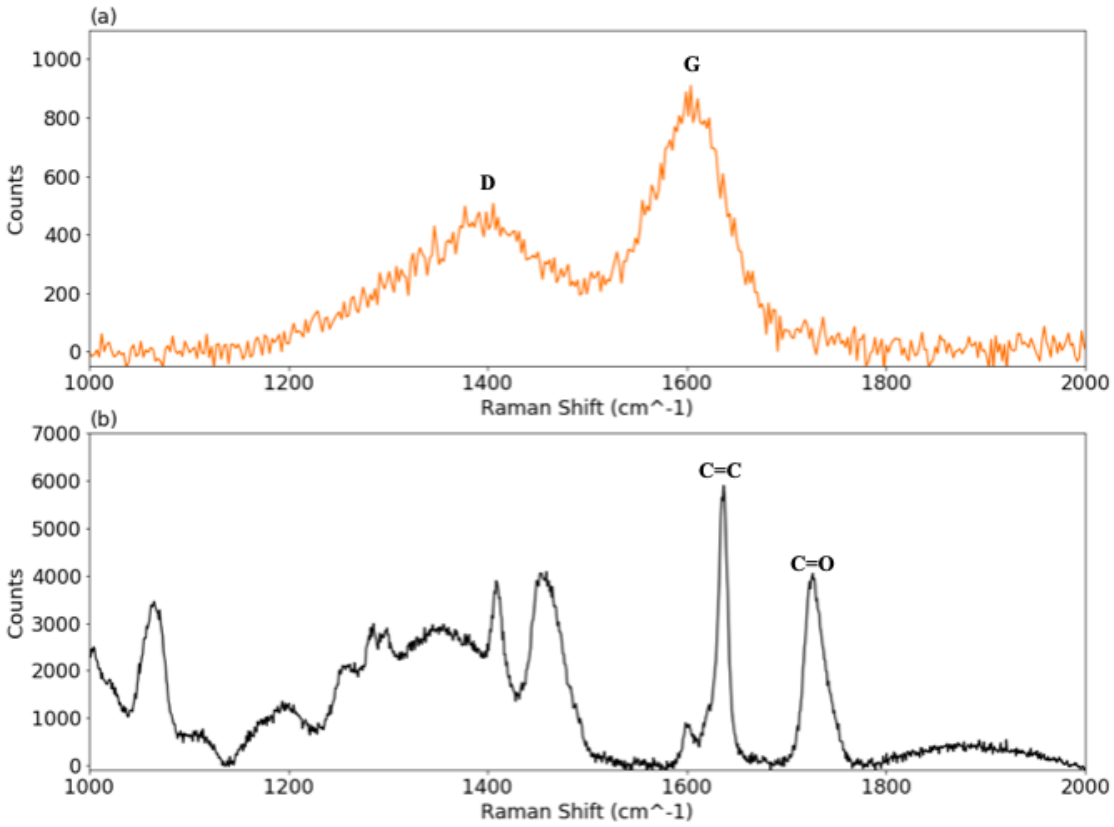

Fig 3.11. Raman spectra of intermediate product (a) from a separate run with step 1 only (RT - 350°C - 2h isothermal process, in air) and polymer bulk sample without any heat treatment (b). In the spectra of the intermediate product, the intensity is much lower because a lower laser power was used to avoid damaging the sample.

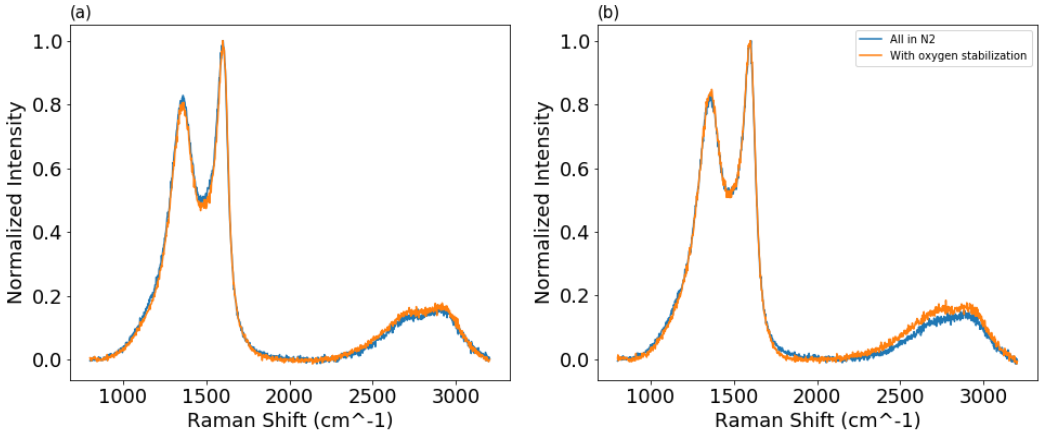

Fig 3.12. Raman spectra on final products after pyrolysis. (a): $H_{350/900}$, (b): $H_{350/950}$.

Summary tables for all heat treatments are given in Table 3.2 and Table 3.3. The weight percent loss of the final carbon products during subsequent heating was used to check the purity. And the Raman peak intensity ratio of D over G band was also included in the tables because increasing I(D)/I(G) is a sign of ordering for disordered carbons and amorphous carbons [22]. For the heat treatments without pre-pyrolysis oxidation, the choice of T1 and T2 doesn't have a significant effect on the final yield of carbon products (ranging from 2.77% to 3.24%). Neither does it have much effect on the weight percent loss during subsequent heating (purity), and Raman peak intensity ratio of D band and G band (crystal ordering). In the case of heat treatments with pre-pyrolysis oxidation, rising T1 to 350 °C from 300°C shows an improvement in the final yield of the carbon products. However, no significant difference in terms of the weight percent loss during subsequent heating and I(D)/I(G). Compared with the heat treatments that were done purely in nitrogen, the pre-pyrolysis oxidation does show an improvement on the final yield, while it doesn't change much on the quality of the final carbon products.

From Table 3.2 and Table 3.3, by maximizing the final yield and minimizing weight loss during subsequent heating, three heat treatments, $H_{300/900}$ (no oxidation process), $H_{350/900}$ (with

oxidation process) were chosen for micropillars. $H_{300/950}$ (with oxidation process) was also chosen as it gives the highest I(D)/I(G) ratio.

Table 3.2. Pyrolysis without oxygen stabilization process (all steps in N_2)

T1 (°C)	W%1	T2(°C)	W%2	W% loss	I(D)/I(G)
300	96.79	900	3.24	5.71	0.83
300	96.95	950	2.77	7.27	0.83
350	86.75	900	3.07	6.64	0.82
350	88.24	950	2.82	6.02	0.84

Table 3.3. Pyrolysis with oxygen stabilization process (step 1 in air)

T1 (°C)	W%1	T2(°C)	W%2	W% loss	I(D)/I(G)
300	79.05	900	7.16	6.42	0.82
300	82.60	950	5.72	6.29	0.85
350	55.59	900	11.56	5.36	0.83
350	61.94	950	9.48	3.99	0.81

(W%1 and W%2 are the weight percent left of the intermediate products and final products respectively. W% loss is the mass loss (%) of final products during subsequent heatings from room temperature to 1000°C in nitrogen. I(D)/I(G) is the absolute Raman peak intensity ratio of D band peak and G band peak for final carbon products)

3.4. Carbonization Process of Micropillars

3.4.1. Micropillars before Pyrolysis

On each wafer that was used for selected heat treatment from section 3.2.3, there is a 5x5 array of pillars for each diameter, 10μm, 25μm, and 50μm. Before pyrolysis, the radii of different pillars were confirmed using an optical microscope, Fig 3.13. The pillars' conditions

were visualized by SEM images of the polymeric micropillars on a sacrificed wafer that were printed with the same parameters, Fig 3.14. From the optical microscope and SEM images, micropillars have the diameters as expected and they well stand on the silicon wafer.

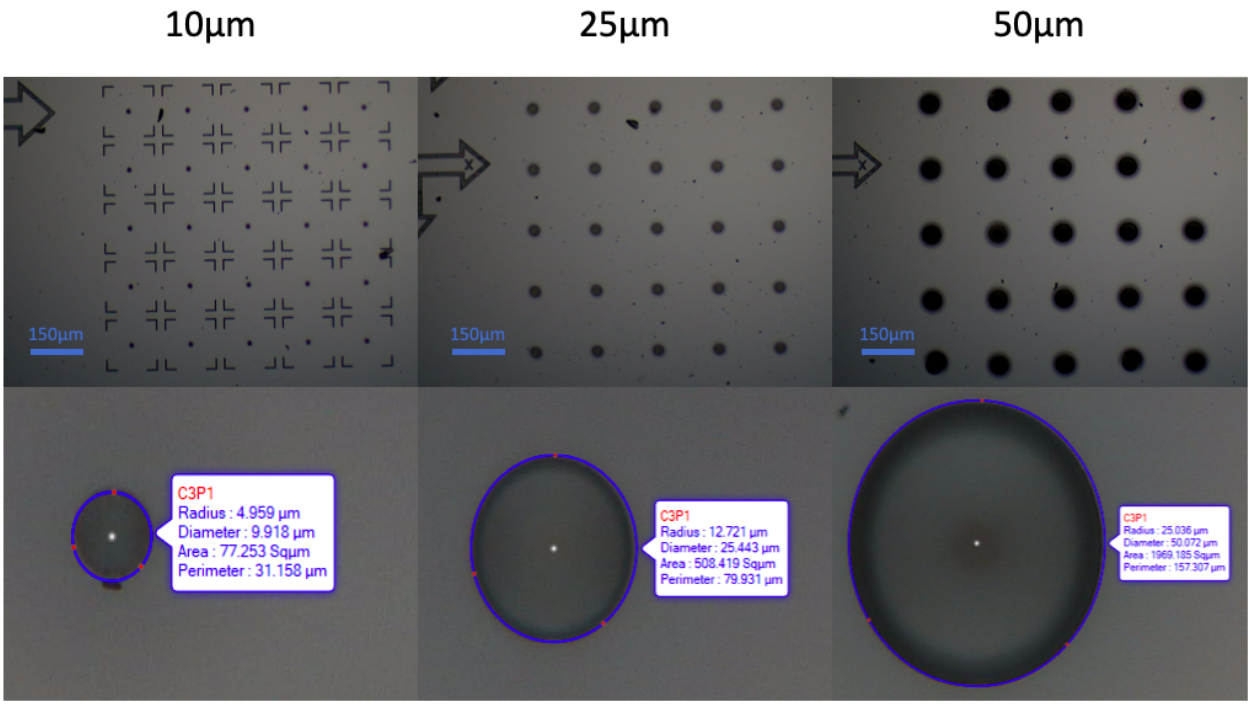

Fig 3.13. Optical microscope image of micropillars. Radii were measured using a built-in measurement tool.

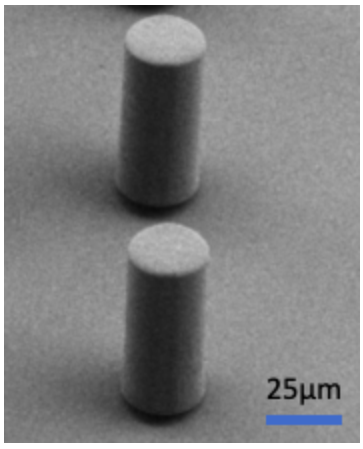

Fig 3.14. SEM image of micropillars with 25µm diameter.

3.4.2. Micropillars after Pyrolysis

Micropillars after pyrolysis with the selected heat treatments from section 3.2.3 were examined using SEM, and Raman spectroscopy. SEM images for micropillars after three heat treatments, $H_{300/900}$ (no oxidation process), $H_{350/900}$ (with oxidation process), and $H_{300/950}$ (with oxidation process), are given in Fig 3.15 - Fig 3.17. For all three heat treatments, the remains of only one array pattern can be identified, and they are most likely to be the array for 50μm pillars after heat treatments. Regardless of the different heat treatments, instead of isotropic shrinkage, only the fragments of pillar structure remain after pyrolysis. This may be a result of traces of oxygen still remaining in the TGA chamber even after nitrogen gas purge, which in such a small volume of polymer can lead to combustion instead of pyrolysis. The different reaction kinetics of pyrolysis and oxidative pyrolysis of polymers have been discussed in the literature [50]. As the goal is to preserve the pre-patterned structures, it is expected that any oxygen traces at high temperatures (eg. 900°C) will be detrimental to the pyrolysis process, especially in volumes as small as the ones in the micropillars fabricated for this work. If future tests determine that in the TGA chamber the presence of oxygen can be eliminated (eg. by purging with nitrogen for multiple hours or apply vacuum before the pyrolysis) and the pyrolysis route that successfully leads to carbonization of the bulk polymer, still does not carbonize the pillars, then this may be a result of size effects and the different diffusion pathways of the volatile degradation fragments in the bulk versus the micropillars. Another issue that requires attention is that micropillars were not well attached to the silicon wafer (see Fig 3.16). This can be improved in future work by precoating the silicon substrates to increase the adhesion.

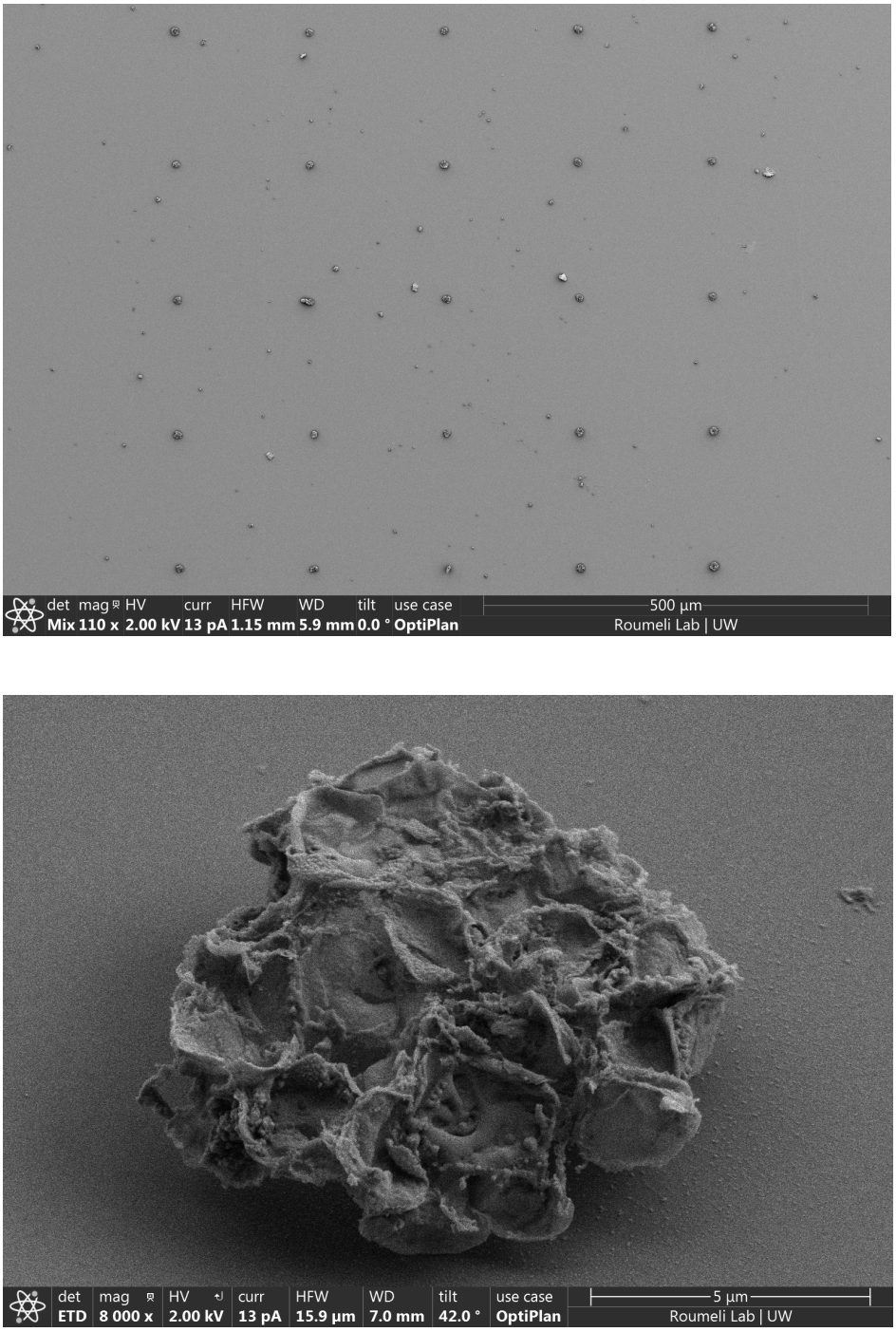

Fig 3.15. SEM images for micropillars after heat treatment $H_{300/900}$ without pre-pyrolysis oxidation.

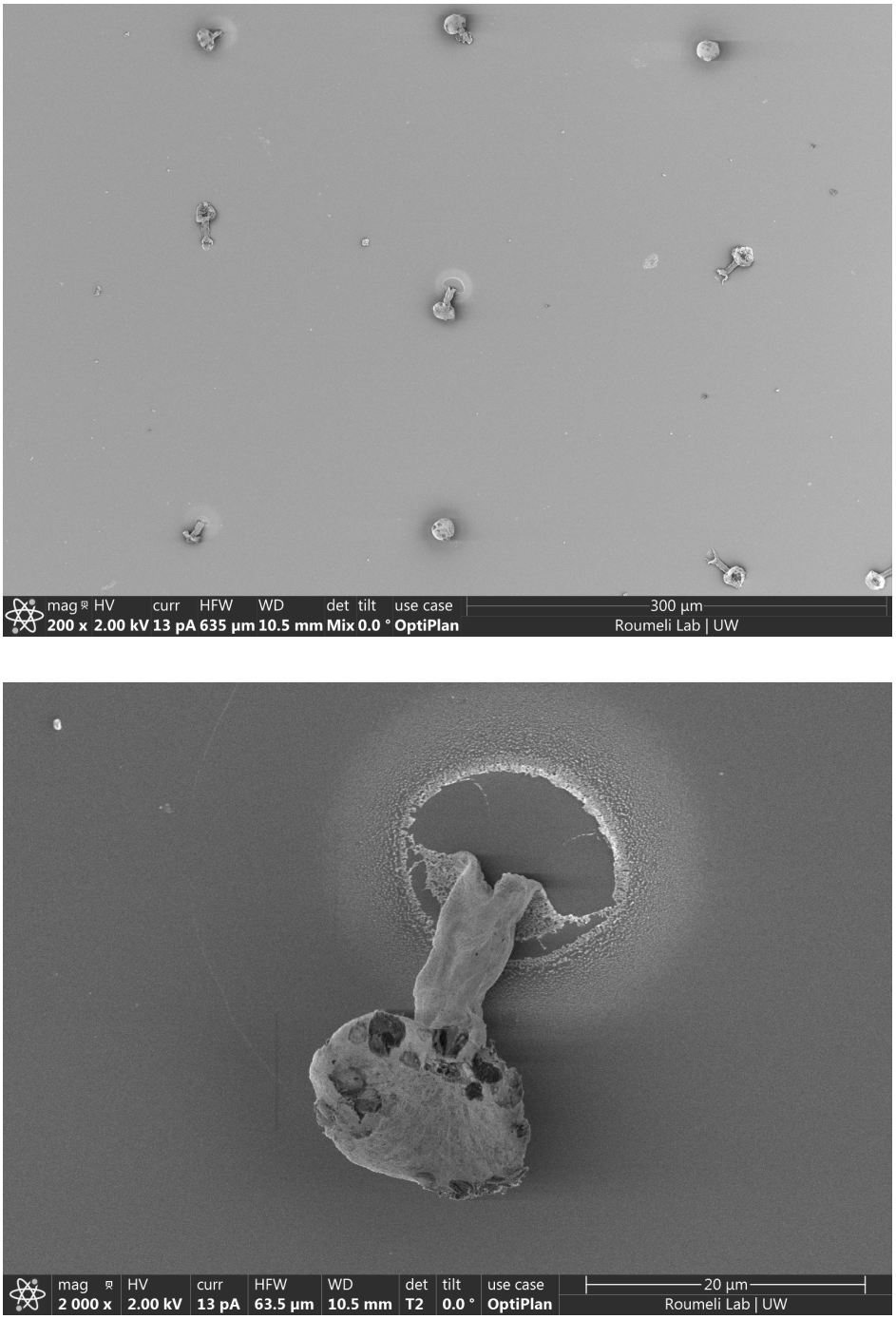

Fig 3.16. SEM images for micropillars after heat treatment $H_{350/900}$ with pre-pyrolysis oxidation.

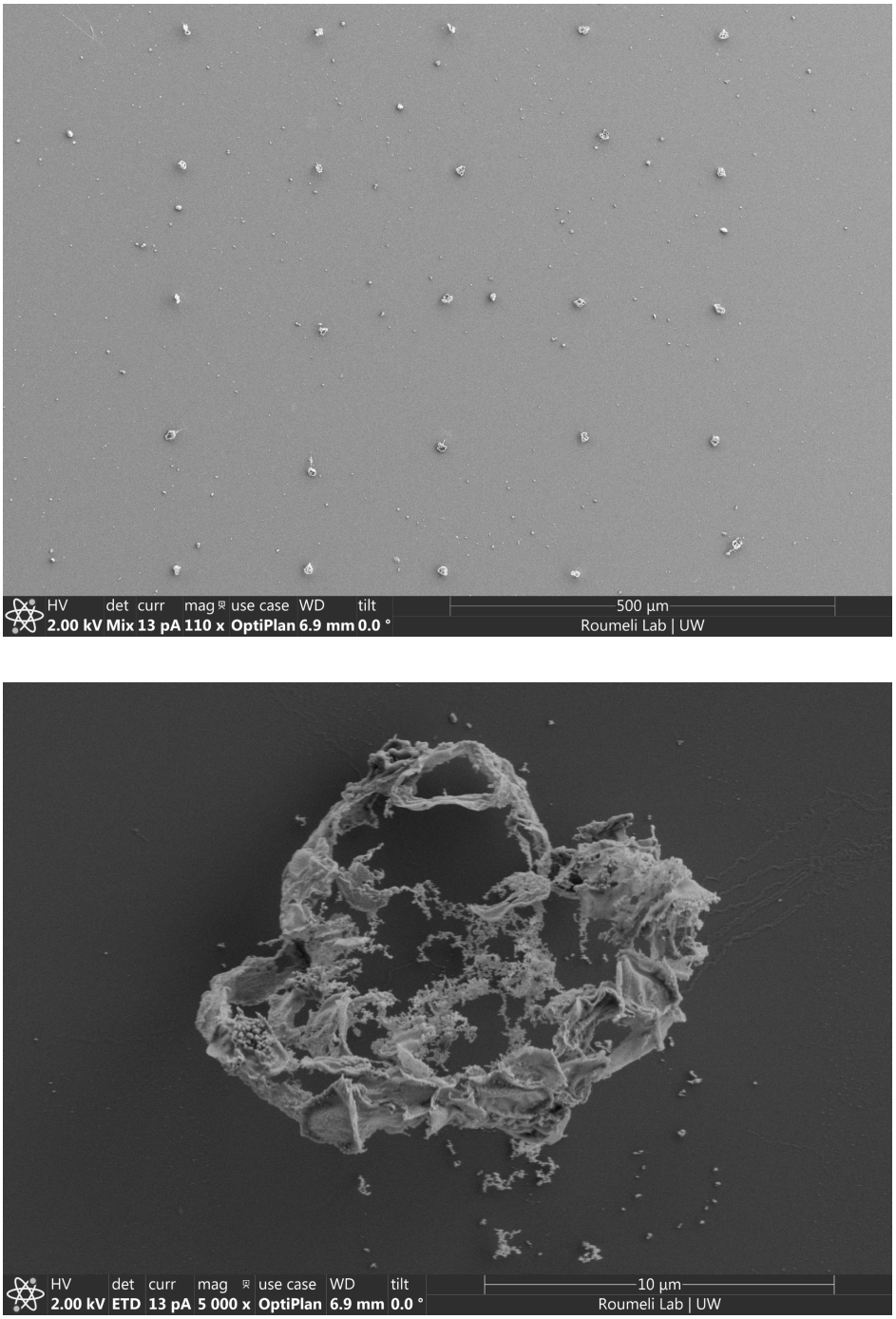

Fig 3.17. SEM images for micropillars after heat treatment $H_{300/950}$ with pre-pyrolysis oxidation.

Though pillar structure was not well preserved regardless of different heat treatments, compared with the other two heat treatments, the remaining structures from $H_{350/900}$ (with pre-pyrolysis oxidation process) appear to be closer to pillar structure. This is consistent with the previous result in the case of the bulk sample, that the $H_{350/900}$ (with pre-pyrolysis oxidation) process is also the heat treatment that gives the best final carbon yield. We also observe that the side of the micropillar shrinks more compared with the top surface resulting in a "mushroom"-like structure (see Fig 3.16), which may be due to the different surface areas of the top/bottom and sides of the pillars (the side surface area of the micropillars, with an aspect ratio of 2, is 8 times larger than the top surface, following $\pi(2r) * (4r)$ *vs* πr^2).

The Raman spectra of the remaining fragments from pyrolyzed micropillars are given in Fig 3.18. While the pre-pyrolysis oxidation process doesn't change much on the quality of the final products from bulk samples, the remaining fragments of the micropillars from heat treatments $H_{300/950}$ (with pre-pyrolysis oxidation) have a lower I(D)/I(G) compared with those from $H_{300/900}$ (pyrolysis only). This may indicate that, in the case of micropillars, the carbon products from $H_{300/900}$ (pyrolysis only) are more ordered and have larger crystallite size, as in amorphous or disordered carbon, a higher D band intensity with respect to G band is a sign of ordering [15][22]. However, this is better to be examined by XRD in future work.

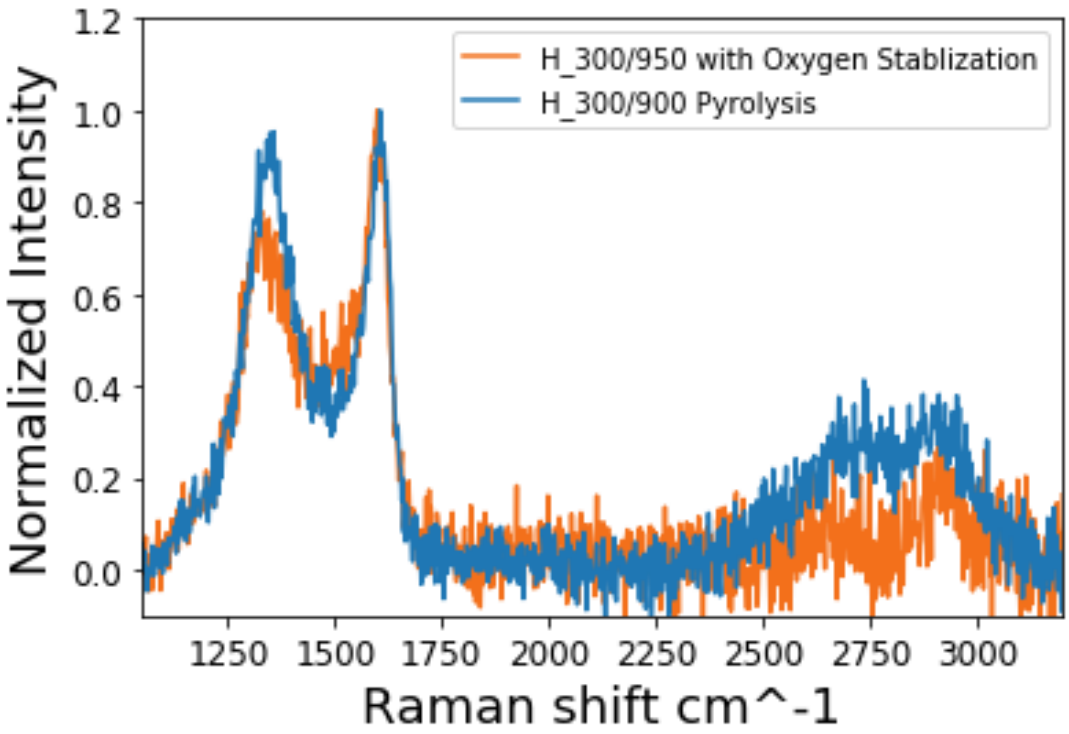

Fig 3.18. Normalized Raman spectra (G band peak intensity = 1) of remaining fragments after heat treatments $H_{300/950}$ (with pre-pyrolysis oxidation) and $H_{300/900}$ (pyrolysis only).

Chapter 4 – Conclusion & Future Work

In this thesis, the final carbon products from multi-step pyrolysis on the custom photoresist, both bulk sample and micropillars, are evaluated. The effect of pre-pyrolysis oxidation on the heat treatments is also investigated.

From the TGA data of different heat treatments with/without oxygen stabilization, in the case of the bulk sample, the pre-pyrolysis oxidation step was shown to improve the final yield of the carbon products, but the quality of the final products is similar in both cases (as examined by Raman spectroscopy and subsequent pyrolysis). In the case of micropillars, structures were not preserved after subjecting them to the same heat treatment as the bulk. Future tests conducted in an oven ensuring lack of oxygen are required to confirm that the same heat treatments may not lead to the same pyrolysis reactions in bulk and microstructures in the custom photoresist. Other analysis that needs to be conducted is XRD measurements and TEM imaging to confirm the crystallite size of final carbon products. Finally, mechanical tests on the micropillars and bulk samples before/after pyrolysis would be required to study the mechanical properties of the initial, intermediate and final products.

References

1. Sharma S. (2018). Glassy Carbon: A Promising Material for Micro- and Nanomanufacturing. Materials (Basel, Switzerland), 11(10), 1857. https://doi.org/10.3390/ma11101857

2. Zhang Y., Zhang L., Zhou C. Review of Chemical Vapor Deposition of Graphene and Related Applications. Acc. Chem. Res. 2013;46:2329–2339. doi: 10.1021/ar300203n.

3. Wang S., Luo Z. Pyrolysis of Biomass. GREEN Alternative Energy Resources; De Gruyter; Science Press; Beijing, China: 2017.

4. Sahota S., Shah G., Ghosh P., Kapoor R., Sengupta S., Singh P., Vijay V., Sahay A., Vijay V.K., Thakur I.S. Review of trends in biogas upgradation technologies and future perspectives. Bioresour. Technol. Rep. 2018;1:79–88. doi: 10.1016/j.biteb.2018.01.002.

5. Bauer J., Schroer A., Schwaiger R., Kraft O. Approaching theoretical strength in glassy carbon nanolattices. Nat. Mater. 2016;15:438–443. doi: 10.1038/nmat4561.

6. G. Seniutinas, A. Weber, C. Padeste, I. Sakellari, M. Farsari, C. David, Beyond 100 nm resolution in 3D laser lithography — Post processing solutions, Microelectronic Engineering, Volume 191, 2018, Pages 25-31, ISSN 0167-9317, https://doi.org/10.1016/j.mee.2018.01.018.

7. Cardenas-Benitez, B., Eschenbaum, C., Mager, D. et al. Pyrolysis-induced shrinking of three-dimensional structures fabricated by two-photon polymerization: experiment and theoretical model. Microsyst Nanoeng 5, 38 (2019). https://doi.org/10.1038/s41378-019-0079-9.

8. Jenkins G.M., Kawamura K. Polymeric Carbons–Carbon Fibre, Glass and Char. Cambridge University Press; Cambridge, UK: New York, NY, USA: 1976.

9. Sharma S., Rostas A.M., Bordonali L., MacKinnon N., Weber S., Korvink J.G. Micro and nano patternable magnetic carbon. J. Appl. Phys. 2016;120:235107. doi: 10.1063/1.4972476.

10. Sharma S., Kumar C.N.S., Korvink J.G., Kübel C. Evolution of Glassy Carbon Microstructure: In Situ Transmission Electron Microscopy of the Pyrolysis Process. arXiv. 2018. 1801.01785.

11. A.R. Bunsell (Ed.), Fibre Reinforcements for Composite Materials, Elsevier Science Publishers (1988), 10.1002/jctb.280480318.

12. Dominique B. Schuepfer, Felix Badaczewski, Juan Manuel Guerra-Castro, Detlev M. Hofmann, Christian Heiliger, Bernd Smarsly, Peter J. Klar, Assessing the structural properties of graphitic and non-graphitic carbons by Raman spectroscopy, Carbon,

Volume 161, 2020, Pages 359-372, ISSN 0008-6223,
https://doi.org/10.1016/j.carbon.2019.12.094.

13. Lehrle R.S. Polymer pyrolysis mechanisms: Experimental approaches for investigating them. J. Anal. Appl. Pyrolysis. 1987;11:55–64. doi: 10.1016/0165-2370(87)85018-0.

14. Sharma S., Sharma A., Cho Y.-K., Madou M. Increased Graphitization in Electrospun Single Suspended Carbon Nanowires Integrated with Carbon-MEMS and Carbon-NEMS Platforms. ACS Appl. Mater. Interfaces. 2012;4:34–39. doi: 10.1021/am2014376.

15. Jurkiewicz, K., Pawlyta, M., Zygadło, D. et al. Evolution of glassy carbon under heat treatment: correlation structure–mechanical properties. J Mater Sci 53, 3509–3523 (2018). https://doi.org/10.1007/s10853-017-1753-7

16. Jenkins G.M., Kawamura K. Structure of Glassy Carbon. Nature. 1971;231:175–176. doi: 10.1038/231175a0.

17. Pesin L., Baitinger E. A new structural model of glass-like carbon. Carbon. 2002;40:295–306. doi: 10.1016/S0008-6223(01)00130-0.

18. Harris P.J.F., Liu Z., Suenaga K. Imaging the atomic structure of activated carbon. J Phys Condens Matter 20:362201–362206 (2008).
https://doi.org/10.1088/0953-8984/20/36/362201

19. Bumbrah G.S., Sharma R.M. Raman spectroscopy – Basic principle, instrumentation and selected applications for the characterization of drugs of abuse, Egyptian Journal of Forensic Sciences, Volume 6, Issue 3, 2016, Pages 209-215, ISSN 2090-536X,
https://doi.org/10.1016/j.ejfs.2015.06.001.

20. Jones, R.R., Hooper, D.C., Zhang, L. et al. Raman Techniques: Fundamentals and Frontiers. Nanoscale Res Lett 14, 231 (2019).
https://doi.org/10.1186/s11671-019-3039-2.

21. Pimenta MA, Dresselhaus G, Dresselhaus MS, Cancado LG, Jorio A, Saito R (2007) Studying disorder in graphite-based systems by Raman spectroscopy. Phys Chem Chem Phys 9:1276–1290. https://doi.org/10.1039/B613962K.

22. Ferrari AC, Robertson J (2000) Interpretation of Raman spectra of disordered and amorphous carbon. Phys Rev B 61:14095–14107.
https://doi.org/10.1103/PhysRevB.61.14095.

23. Tuinstra F, Koenig JL (1970) Raman spectrum of graphite. J Chem Phys 53:1126–1130.
https://doi.org/10.1063/1.1674108.

24. Garion C. Mechanical Properties for Reliability Analysis of Structures in Glassy Carbon. World J. Mech. 2014;4:79–89. doi: 10.4236/wjm.2014.43009.

25. Fischbach D.B. Magnetic susceptibility of glassy carbon. Carbon. 1967;5:565–570. doi: 10.1016/0008-6223(67)90034-6.

26. Walker P.L. Chemistry and Physics of Carbon: A Series of Advances. Volume 16. Marcel Dekker, Inc.; New York, NY, USA: Basel, Switzerland: 1981.

27. Jenkins G.M., Kawamura K. Polymeric Carbons–Carbon Fibre, Glass and Char. Cambridge University Press; Cambridge, UK: New York, NY, USA: 1976.

28. Reichmanis E., Houlihan F.M., Nalamasu O., Neenan T.X. Chemical Amplification Mechanisms for Microlithography. In: Thompson L.F., Willson C.G., Tagawa S., editors. Polymers for Microelectronics. Volume 537. American Chemical Society; Washington, DC, USA: 1993. pp. 2–24.

29. Vilčáková J., Kutějová L., Jurča M., Moučka R., Vícha R., Sedlačík M., Kovalcik A., Machovský M., Kazantseva N. Enhanced Charpy impact strength of epoxy resin modified with vinyl-terminated polydimethylsiloxane: Research Article. J. Appl. Polym. Sci. 2018;135:45720. doi: 10.1002/app.45720.

30. Anthony R., Laforge E., Casey D.P., Rohan J.F., O'Mathuna C. High-aspect-ratio photoresist processing for fabrication of high resolution and thick micro-windings. J. Micromech. Microeng. 2016;26:105012. doi: 10.1088/0960-1317/26/10/105012.

31. Hancox R.N., Lamb G.D., Lehrle R.S. Sample size dependence in pyrolysis: An embarrassment, or a utility? J. Anal. Appl. Pyrolysis. 1991;19:333–347. doi: 10.1016/0165-2370(91)80054-C.

32. Warner, S.B., Peebles, L.H. & Uhlmann, D.R. Oxidative stabilization of acrylic fibres. J Mater Sci 14, 556–564 (1979). https://doi.org/10.1007/BF00772714

33. Gergin, İ., Ismar, E., & Sarac, A. S. (2017). Oxidative stabilization of polyacrylonitrile nanofibers and carbon nanofibers containing graphene oxide (GO): a spectroscopic and electrochemical study. Beilstein journal of nanotechnology, 8, 1616–1628. https://doi.org/10.3762/bjnano.8.161

34. Cho M., Ko K.F., Renneckar S. Impact of Thermal Oxidative Stabilization on the Performance of Lignin-Based Carbon Nanofiber Mats. ACS Omega 2019 4 (3), 5345-5355 DOI: 10.1021/acsomega.9b00278

35. Donnet J.-B., editor. Carbon Fibers. 3rd ed. Marcel Dekker; New York, NY, USA: 1998.

36. V. Harinarayana, Y.C. Shin, Two-photon lithography for three-dimensional fabrication in micro/nanoscale regime: A comprehensive review, Optics & Laser Technology, Volume 142, 2021, 107180, ISSN 0030-3992, https://doi.org/10.1016/j.optlastec.2021.107180.

37. C.B. Arnold, A. Piqué. Laser Direct-Write Processing, MRS Bulletin, 32 (2007), pp. 9-15

38. S. Kawata, H.B. Sun, T. Tanaka, K. Takada. Finer features for functional microdevices, Nature, 412 (2001), pp. 697-698

39. En-Shinn Wu, James H. Strickler, W. R. Harrell, and Watt W. Webb "Two-photon lithography for microelectronic application", Proc. SPIE 1674, Optical/Laser Microlithography V, (1 June 1992); https://doi.org/10.1117/12.130367

40. Q. Hu,"Multiphoton Lithograpy Based 3D Micro/Nano Printing," EPSRC Centre for Innovative Manufacturing in Additive Manufacturing 1–30. PowerPoint Presentation (ncl.ac.uk).

41. Fischer, J. & Wegener, M. Three-dimensional direct laser writing inspired by stimulated-emission-depletion microscopy. Opt. Mater. Express 1, 614–624 (2011)

42. Lim, Y., Heo, J., Madou, M. & Shin, H. Monolithic carbon structures including suspended single nanowires and nanomeshes as a sensor platform. Nanoscale Res. Lett. 8, 492 (2013).

43. VanDersarl J.J., Mercanzini A., Renaud P. Integration of 2D and 3D Thin Film Glassy Carbon Electrode Arrays for Electrochemical Dopamine Sensing in Flexible Neuroelectronic Implants. Adv. Funct. Mater. 2015;25:78–84. doi: 10.1002/adfm.201402934.

44. Mohamed Hassan Y., Caviglia C., Hemanth S., Mackenzie D.M.A., Petersen D.H., Keller S.S. Pyrolytic carbon microelectrodes for impedance based cell sensing. ECS Trans. 2016;72:35–44. doi: 10.1149/07201.0035ecst.

45. Thiha A., Ibrahim F., Muniandy S., Dinshaw I.J., Teh S.J., Thong K.L., Leo B.F., Madou M. All-carbon suspended nanowire sensors as a rapid highly-sensitive label-free chemiresistive biosensing platform. Biosens. Bioelectron. 2018;107:145–152. doi: 10.1016/j.bios.2018.02.024.

46. Juodkazis, S., Mizeikis, V., Seet, K. K., Miwa, M. & Misawa, H. Two-photon lithography of nanorods in SU-8 photoresist. Nanotechnology.

47. Mishra, R., Pramanick, B., Maiti, T. K. & Bhattacharyya, T. K. Glassy carbon microneedles—new transdermal drug delivery device derived from a scalable C-MEMS process. Microsyst. Nanoeng. 4, 38 (2018).

48. Oakdale JS, Ye J, Smith WL, Biener J. Post-print UV curing method for improving the mechanical properties of prototypes derived from two-photon lithography. Opt Express. 2016 Nov 28;24(24):27077–86.

49. Jiang LJ, Zhou YS, Xiong W, Gao Y, Huang X, Jiang L, et al. Two-photon polymerization: investigation of chemical and mechanical properties of resins using Raman microspectroscopy. Opt. Lett. 39, 3034-3037 (2014).

50. Vinu R, Broadbelt LJ. Unraveling reaction pathways and specifying reaction kinetics for complex systems. Annu Rev Chem Biomol Eng. 2012;3:29-54. doi: 10.1146/annurev-chembioeng-062011-081108. Epub 2012 Jan 13. PMID: 22468596.